THE JOURNAL OF PHYSICAL CHEMISTRY C

Article

pubs.acs.org/JPCC

Enhancement of Electronic and Optical Properties of ZnO/Al_2O_3 Nanolaminate Coated Electrospun Nanofibers

Roman Viter,[*,†,⊥] Igor Iatsunskyi,[*,‡] Viktoriia Fedorenko,[§,∥] Saulius Tumenas,[⊥] Zigmas Balevicius,[⊥,#] Arunas Ramanavicius,[⊥] Sebastien Balme,[§] Mateusz Kempiński,[‡] Grzegorz Nowaczyk,[‡] Stefan Jurga,[‡,¶] and Mikhael Bechelany[*,§]

[†]Institute of Atomic Physics and Spectroscopy, University of Latvia, 19, Raina Blvd., LV 1586 Riga, Latvia

[‡]NanoBioMedical Centre, Adam Mickiewicz University, 85 Umultowska str., 61-614 Poznan, Poland

[§]Institut Européen des Membranes, UMR 5635 ENSCM UM CNRS, Université Montpellier, Place Eugene Bataillon, F-34095 Cedex 5 Montpellier, France

[∥]Faculty of Physics, Experimental physics department, Odessa National I.I. Mechnikov University, 42, Pastera, 65026 Odessa, Ukraine

[⊥]State Research Institute Center for Physical Sciences and Technology, Savanoriuave. 231, LT-01108 Vilnius, Lithuania

[#]Faculty of Electronics, Vilnius Gediminas Technical University, Sauletekio 11, LT-10223 Vilnius, Lithuania

[¶]Department of Macromolecular Physics, Adam Mickiewicz University, 85 Umultowska str., 61-614 Poznan, Poland

Supporting Information

ABSTRACT: Nanolaminates are new class of promising nanomaterials with outstanding properties. Here we explored on the tuning of structural properties and the enhancement of electronic and optical properties of 1D PAN ZnO/Al_2O_3 nanolaminates designed by atomic layer deposition (ALD) and electrospinning. The influence of ZnO/Al_2O_3 bilayer thicknesses on the fundamental properties of 1D PAN ZnO/Al_2O_3 nanolaminates has been investigated. Due to the quantum confinement effect, the shift of XPS peaks to higher energies has been observed. Work function of Al_2O_3 was mostly independent of the bilayers number, whereas the ZnO work function decreased with an increase of the bilayer number. Photoluminescence of the 1D PAN ZnO/Al_2O_3 nanolaminates corresponded to emission bands in ZnO nanolayers. Due to quantum confinement and surface band bending, no excitonic peaks were observed. The defect emission band was affected by the band bending and defect concentration. The enhanced photoluminescence of the 1D PAN ZnO/Al_2O_3 nanolaminates allows applications in optical (bio)sensing field.

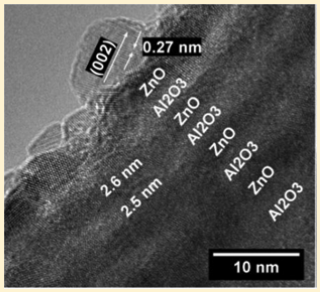

INTRODUCTION

Nanolaminates are new class of promising nanomaterials with well-tailored properties. These materials are obtained by alternating layers with an individual thickness on the nanometer scale of different materials.[1] They manifest outstanding advanced mechanical,[2] electrical, and optical properties[1] which depend from the constituent materials forming these nanolaminates. Zinc Oxide (ZnO) which can be incorporated in the nanolaminate material is a n-type semiconductor with wide band gap value (3.3 eV) and high exciton binding energy (0.06 eV). It also exhibited room temperature photoluminescence in UV−vis region.[1,3] Among the different techniques to elaborate oxides based nanolaminates, atomic layer deposition (ALD) is a powerful tool to fabricate different oxide materials.[4,5] It is based on two self-limiting surface reactions which allow growing continuous, smooth, and conformal ultrathin film on high aspect ratio and complex substrates such as the 1D nanotructures with a precise dimensional control. This paper deals with the investigation of electronic and optical properties of ZnO/Al_2O_3 nanolaminate coated electrospun nanofibers.

The design of Al_2O_3/ZnO nanolaminates as well as ZnO thin film doped with Al was widely investigated by ALD.[2,6−9] The ZnO deposited on Al_2O_3 thin films in the Al_2O_3/ZnO nanolaminates demonstrated a different growth direction in comparison to single ZnO thin film.[10] ZnO demonstrates as well a change from amorphous to nanocrystalline with the increase of the bilayers thickness where Al_2O_3 layer remains amorphous.[2] The change of the growth direction, the crystallinity, and the Al doping influence the optical,[1,11] electrical,[12] and mechanical properties[2] of the deposited thin films. Recently, we investigated the optical and the structure properties of ZnO/Al_2O_3 nanolaminates deposited on Si substrates by ALD.[1] We demonstrated the amorphous-to-crystalline phase transitions of ZnO in ZnO/Al_2O_3 nanolaminates as well as the quantum confinement and size dependent room temperature photoluminescence.[1] It was shown a correlation between structure (grain size and layer thickness) and optical (extinction coefficient and refractive

Received: December 15, 2015
Revised: February 19, 2016
Published: February 19, 2016

DOI: 10.1021/acs.jpcc.5b12263
J. Phys. Chem. C 2016, 120, 5124−5132

index), pointing to the influence of growth conditions on the fundamental properties of the nanolaminates.[1]

Different 1D nanostructures such as carbon nanotubes (CNTs) and polymer fibers have been investigated in order to design core/shell nanostructures using ALD of metal oxides.[13−17] Different studies were performed for the growth of oxides of Carbon nanotubes. Stano et al. reported the influence of CNTs type and the defect concentration on the ALD coating.[17] For low defect concentration, ALD coating cannot be realized. The functionalization of CNTs surface is needed to promote the nucleation of the oxide film. Carboxyl and hydroxyl groups are formed on the CNTs surface to initiate the ALD growth. Kemnade et al. showed that conformal growth of ALD ZnO layer on CNTs requested the modification of the CNTs with aromatic linking agents.[14] Lin et al. reported on the importance of CNT functionalization before deposition of ZnO nanolayers by ALD.[15] Kayaci et al. reported that ALD ZnO layers provided a conformal coating of nylon fibers.[13] However, Oldham et al. demonstrated that TMA and DEZ precursors could chemically react with polyamide-6 (PA-6) nylon nanofibers destroying their physical properties.[16] Therefore, the conformal and uniform ALD coating on 1D nanostructures could be achieved by the right choice of the core chemical composition and surface state of the 1D nanostructures. PAN nanofibers are good chemically stable material for 1D core/shell nanostructure design.[18] PAN nanofibers have been successfully used for chemical deposition of different metal nanoparticles on their surface. It was shown that PAN nanofibers have good mechanical and thermal stability. The adsorption sites present on the surface of the PAN fibers would facilitate the nucleation of the metal oxide layers by ALD. Thus, integration of metal oxide ALD technique and PAN nanofibers has a good perspective.

Previously, we have reported on the fabrication of three-dimensional polyacrylonitrile/ZnO material prepared by the combination of electrospinning and atomic layer deposition (ALD) as new material with large surface area to enhance the optical properties.[19,20] The study of room temperature photoluminescence (PL) spectrum exhibits peak intensity which enhance by a factor of 2000 compared to a flat Si substrate.[20] In the present work, we report on the enhancement of electronic and optical properties of 1D organic core with ZnO/Al_2O_3 nanolaminates shell nanostructures. The influence of structure parameters of ZnO/Al_2O_3 nanolaminates (thickness, grain size, number of bilayers, defect concentration) on the main electronic (work function) and optical (photoluminescence and band gap) properties will be discussed. The enhancement of electronic and optical properties will allow application in different fields such sensors and biosensors.

MATERIALS AND METHODS

Polyacrylonitrile (PAN) nanofibers have been elaborated by electrospinning technique to be a template for the nanolaminates design by ALD.

1. Electrospinning of PAN Nanofibers. Polyacrylonitrile PAN (M_w = 150 000) and dimethylformamide (ACS reagent, ≥99.8%) were purchased from Sigma-Aldrich. Polyacrylonitrile (10 wt % PAN) was dissolved in dimethylformamide (DMF). The electrospinning solution was maintained under agitation for 1 h and then heated in an oil bath at 80 °C for 10 min. The used electrospinning machine was a homemade device using an HPx 600 605 generator (physical instruments) and a KDS 100 syringe pump. The polymer solution was electrospuned in ambient air atmosphere under an applied voltage of 25 kV with a flow rate of 3 mL h^{-1} using a 0.7 mm diameter syringe connected to the positive output of the generator. A fix collector was placed 25 cm from the tip of the syringe and was related to the negative output of the generator. The droplet was transformed to a Taylor cone due to the electrostatic field applied between the syringe and the collector. The evaporation of the solvent during the process induces the formation of a net of submicron fiber.

2. ALD Deposition of Nanolaminates. Diethyl zinc (DEZ) ($Zn(CH_2CH_3)_2$, 95% purity, CAS: 557-20-0) and trimethylaluminum (TMA) ($(CH_3)_3Al$) 98% purity, CAS: 75-24-1) were purchased from Sigma-Aldrich. A custom-made ALD reactor was used for the synthesis of ultrathin Al_2O_3/ZnO nanolaminates. ALD was performed using sequential exposures of TMA (DEZ) and H_2O separated by a purge of Argon with a flow rate of 100 sccm. The deposition regime for ZnO and Al_2O_3 consisted of 0.2 s pulse of TMA (DEZ), 30 s of exposure to TMA (DEZ), 30 s of purge with argon followed by 2 s pulse of H_2O, 30 s of exposure to H_2O, and finally 40 s purge with argon. Al_2O_3/ZnO ultrathin nanolaminates with different numbers of cycles were deposited on electrospun PAN nanofibers (Table 1). The deposition temperature was fixed to 100 °C. We note here that, in contrast to the deposition of thin films on flat surfaces, the reactants had to diffuse into the high-aspect-ratio structures. Therefore, an exposure time should be added and adapted in order to ensure the conformal coating of the PAN nanofibers. GPC of ∼0.2 nm/cycle has been observed for Al_2O_3 and ZnO. These values are consistent with what has been reported elsewhere by Karvonen et al.[9] on ZnO/Al_2O_3 nanolaminates. The difference between the GPC of Al_2O_3 reported on single Al_2O_3 layers and the ZnO/Al_2O_3 nanolaminates has been attributed to the higher surface area of the rough crystalline ZnO interfaces.[9]

Table 1. Al_2O_3/ZnO Ultrathin Nanolaminates Synthesis by ALD

samples	cycles of Al_2O_3	cycles of ZnO	no. of bilayers	bilayer thickness (nm)
Al_2O_3/ZnO 20 (0.6/0.6 nm)	3	3	20	1.2
Al_2O_3/ZnO 10 (1/1 nm)	5	5	10	2
Al_2O_3/ZnO 4 (2.6/2.6 nm)	13	13	4	5.2
Al_2O_3/ZnO 2 (5/5 nm)	25	25	2	10
Al_2O_3/ZnO 1 (10/10 nm)	50	50	1	20

3. Structural, Chemical, and Optical Characterizations. Structural and chemical compositions of all PAN-nanolaminates were analyzed by transmission electron microscopy (TEM). Images were obtained with a JEOL ARM 200F high-resolution transmission electron microscope (200 kV) with an EDX analyzer (JED2300, at least 30 accumulations, matrix 512 × 512 points in STEM mode). Dark and bright field detectors were used.

FTIR spectra were obtained with the Bruker VERTEX 70v vacuum spectrometer using the RT-DLaTGS detector (spectral resolution of 4 cm^{-1}). X-ray diffraction measurements were performed with PANAlytical Xpert-PRO diffractometer equipped with a X'celerator detector using Ni-filtered Cu-radiation. Surface structural and chemical properties of PAN-nano-

DOI: 10.1021/acs.jpcc.5b12263
J. Phys. Chem. C 2016, 120, 5124−5132

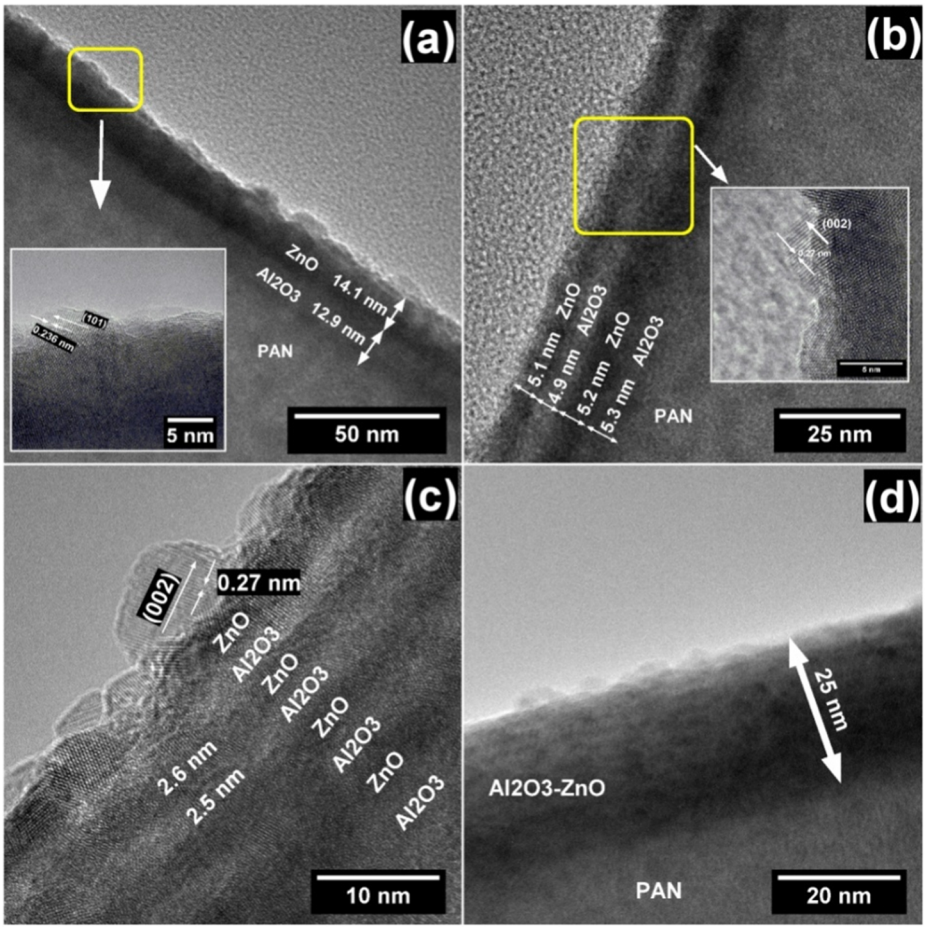

Figure 1. TEM images of PAN-Al_2O_3/ZnO nanolaminates with different bilayers thicknesses: (a) 20 nm, (b) 10 nm, (c) 5.2 nm, and (d) 2 nm. Insets show the corresponding high-magnification images.

laminates were analyzed by means of the XPS/UPS technique mounted within the Omicron Nanotechnology multiprobe UHV system, using a monochromatized Al Kα X-ray as the excitation source ($h\nu$ = 1486.6 eV) and choosing C 1s (284.6 eV) as the reference line. XPS was conducted under ultrahigh vacuum (10^{-7} Pa). CasaXPS software was used to analyze the XPS data. Optical properties of ultrathin nanolaminates have been studied by photoluminescence spectroscopy (in the spectral range of 370−800 nm). The excitation of luminescence was performed by a solid state laser source (Nd:YAG, 355 nm, 13 mW cm^{-2}). The registration of the emitted spectra was provided by an experimental setup described elsewhere.[1,3,20]

RESULTS AND DISCUSSION

1. Chemical and Structural Characterizations. TEM images of PAN-Al_2O_3/ZnO nanostructures are presented in Figure 1 (TEM image of the end face of PAN fiber and TEM/EDX mapping in Supporting Information (Figures SI1 and SI2)). The TEM images confirm the conformal coating of the PAN nanofibers by ALD. It is clearly seen the nanolaminates formation (ZnO (dark stripes) and Al_2O_3 (light stripes)). The total thickness of nanolaminates layer is 25 nm (Figure 1d). Lattice fringes seen in high-resolution TEM images reveal ZnO nanocrystals with (101) and (002) planes (Figure 1a and b insets). Using ImageJ software, the grain size and the interplane distances for (101) and (002) lattice planes were calculated (insets of Figure 1a−c). The grain size was calculated using elliptical shape fitting and the longer axis was used as the grain size. The average grain size for 20 nm, 10 and 5.2 nm bilayer thicknesses were 9.8 ± 2.5 nm, 6.5 ± 1.5 nm and 5.3 ± 2.1 nm, respectively. For 2 and 1.2 bilayer thicknesses, the grain size was not determined due to the quality of the image and the resolution of TEM. We suppose that the in case of 20, 10, and 5.2 nm bilayer thicknesses, the grains were elongated and limited by the layer thickness. The TEM analysis provided evidence that the Al_2O_3 layers are amorphous for all samples. The ZnO layers are in a polycrystalline phase. The TEM images demonstrate the ability to produce highly uniform layers of nanolaminates covered PAN fibers by the ALD processes.

The Fourier-transform infrared (FTIR) absorbance spectrum is presented in Figure 2a. The FTIR data reveals a presence of the main vibration bands of polyacrylonitrile (PAN) in investigated samples. The bands manifest themselves in the ranges of 2260−2240 cm^{-1} (C≡N stretch) and 1485−1035 cm^{-1} (C−O and C−C stretch and aliphatic CH-group vibrations of different modes in CH, CH_2 and CH_3). Very sharp and strong peak at 2243 cm^{-1} is assigned to nitrile band. After deposition of Al_2O_3/ZnO nanolaminates, two new bands appear in the 1670−1600 cm^{-1} spectral range which are attributed to carbonyl group vibrations.[21] In the spectral range 600−380 cm^{-1}, the peak at 407 cm^{-1} is visible, which is related to ZnO $E_{1,TO}$ phonon mode. With a decrease of the nanolaminate thickness, the ZnO phonon related absorption decreases, and at the 1.2 nm bilayer thickness it is undetectable. This tendency implies the transition from the polycrystalline to

DOI: 10.1021/acs.jpcc.5b12263
J. Phys. Chem. C 2016, 120, 5124−5132

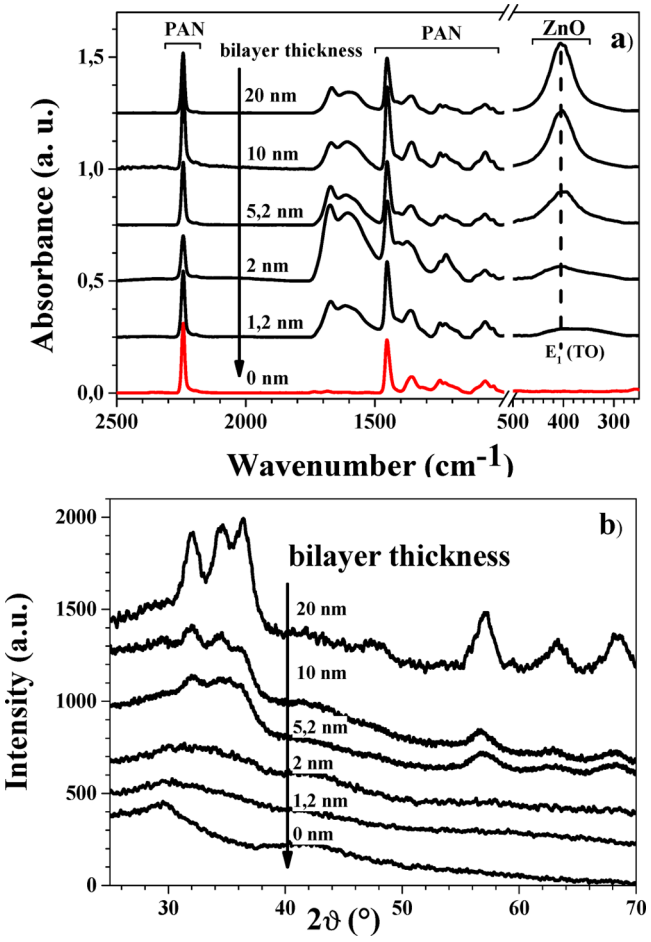

Figure 2. (a) Absorbance spectra and (b) XRD spectra of PAN-Al_2O_3/ZnO nanolaminates at various bilayers thicknesses. Spectra are shifted for clarity.

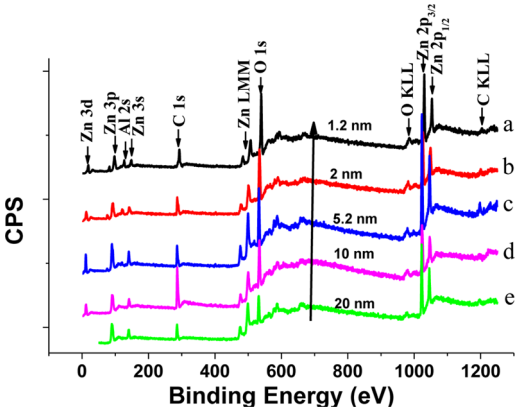

Figure 3. XPS survey spectra of ZnO/Al_2O_3 nanolaminates coated polymer fiber with different bilayer thicknesses: (a) 1.2 nm, (b) 2 nm, (c) 5.2 nm, (d) 10 nm, and (e) 20 nm. Main core levels are labeled. Data are normalized to each O 1s peak maximum and separated vertically.

amorphous phase of the nanolaminates with low bilayer thicknesses. Similar tendency is show by XRD spectra recorded from nanolaminates with the same bilayer thicknesses (Figure 2b). The ZnO related XRD peaks essentially decrease with a decrease of bilayer thickness. It is reasonable to assume that amorphous nature of ultrathin nanolaminates required minimum thickness to allow crystallization in a thin film.[11] The proposed crystallization model for ultrathin layers and superlattices is taking into account the interface energies, the thickness of the layers, the melting point of the system, and the bulk amorphous crystallization temperature.[22] It was shown that exponential increase of the crystallization temperature leads to the decrease of the minimal thickness at which crystallization occurs. From XRD (Figure 2b), HRTEM, and previous studies,[2,11] this bilayer thickness value was shown to be 2.5 nm for Al_2O_3/ZnO nanolaminates. So, we assume that close to this value is the point at which the crystallization process starts in Al_2O_3/ZnO nanolaminates. The ZnO grain size decreases with decreasing the bilayer thickness. The amorphous Al_2O_3 layer play the role of stopping layer for ZnO growth. The ZnO layer is forced to renucleate on the underlying amorphous Al_2O_3 layer inducing the decrease of the grain size when the bilayer thickness decreases.

The surface composition and chemical state polymer fiber coated with different bilayers thicknesses of ZnO/Al_2O_3 nanolaminates were studied by XPS (Figure 3). Samples depict zinc (Zn), aluminum (Al), oxygen (O), and carbon (C) components. It is worth to say that no peaks, related to Al were observed for nanolaminates with 10 and 20 nm bilayer thicknesses (Figure 3d and e). It is related to the limit of the penetration depth of the excitation X-ray photons. As was shown in our previous work, the Auger parameter is a useful tool to determine the stoichiometry and the phase of obtained structures.[23] The main peak of the Zn (LMM) Auger series occurs at kinetic energy of 988 ± 0.5 eV. From this value and Zn $2p_{3/2}$ binding energy, we calculated the modified Auger parameter α' (α' = BE(Zn $2p_{3/2}$)+KE(Zn LMM), where BE and KE are a binding energy of the core level $2p_{3/2}$ and a kinetic energy of the Auger transition involving electrons from L3, M45, and M45 core levels) as defined by Wanger. For all samples, our calculations lead to a value of 2009.9 ± 0.5 eV corresponding to ZnO (wurtzite).[24] This indicates the formation of stoichiometric ZnO in all samples.

As the studied samples had a single ZnO layer thickness from 0.6 to 10 nm, their fundamental properties would change from the bulk materials to nanoscale.[25] In order to understand the surface role and quantum confinement effects, the energy ranges related to Zn and O lines were rescaled and analyzed. Figure 4 shows the core level of the Zn 2p spectra. The core level binding energies of Zn $2p_{3/2}$ and Zn $2p_{1/2}$ are about 1022.5 ± 0.1 and 1045.6 ± 0.1 eV (20 nm bilayer thickness). These peaks indicate the presence of ZnO phase.[26−29] The binding energy difference (duplet) between these components is about 23.1 ± 0.1 eV which could be attributed to the Zn^{2+} ions in ZnO. From Figure 4, we can see the shift of peak positions to higher energies with the decrease of bilayer thickness. However, the difference of 23.1 eV in all samples indicates the presence of the normal state of Zn^{2+} in the ZnO. The oxygen core level peak behaves similarly (Figure 4 bottom image). The observed phenomenon of XPS size shift can be explained, by growth of surface to volume atoms relation and correspondingly relative increase of dangling bonds on the surface. This leads to change of electronic structure in nanocrystals, resulting in increase of binding energies.[23,25,30]

The XPS peaks were analyzed by deconvolution of peaks using CasaXPS software (Supporting Information Figure SI3). It was found that Zn $2p_{1/2}$ peak of 1.2 nm bilayer thickness sample was well fitted with one peak, centered at 1045 eV, whereas other samples showed two peak fittings of the

DOI: 10.1021/acs.jpcc.5b12263
J. Phys. Chem. C 2016, 120, 5124−5132

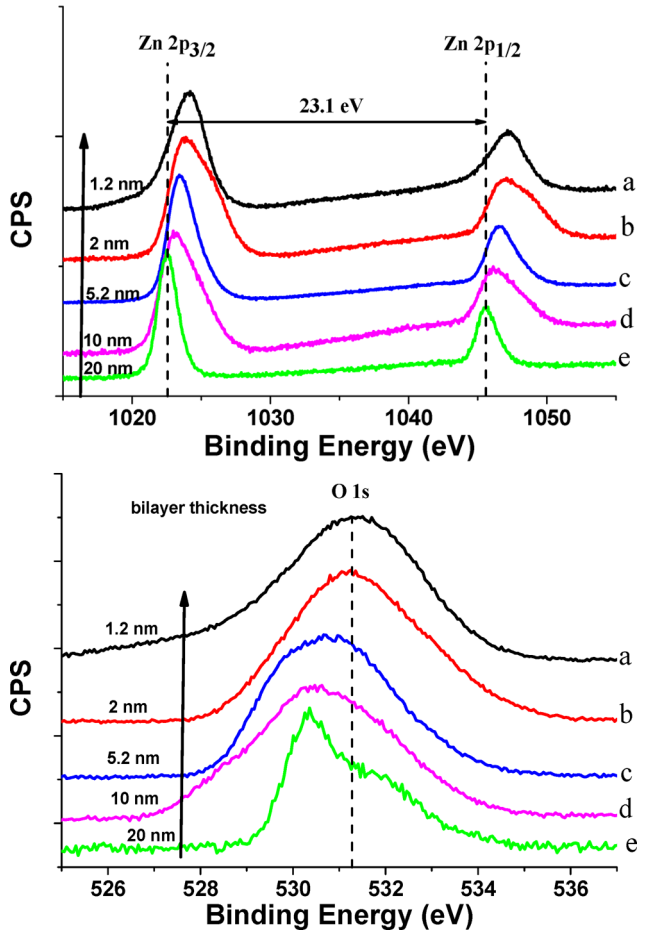

Figure 4. XPS survey spectra of ZnO/Al_2O_3 nanolaminates coated polymer fiber with different bilayers thicknesses: (a) 1.2 nm, (b) 2 nm, (c) 5.2 nm, (d) 10 nm, and (e) 20 nm. Main core levels are labeled. Data are normalized and separated vertically.

corresponding Zn $2p_{1/2}$ peak. The obtained peaks P1 and P2 were in the range of 1045 ± 0.6 eV and 1044 ± 0.6 eV, respectively. The ratio of Zn $2p_{1/2}$ (P2)/(P1) increased with a growth of a bilayer thickness, pointing to the decrease of surface-to-volume aspect ratio. The analysis of Zn $2p_{1/2}$ peaks showed similar results: the main peak was shifted toward lower energies and additional peak at 1022.3 ± 0.6 eV appeared in the spectra, pointing to the presence of Zn species (interstitials) or Zn−OH in ZnO.[31]

Analysis of O 1S peak has been fitted with three peaks, centered at 529.6 ± 0.5 (P1), 531.3 ± 0.2 (P2) and 532.1 ± 0.4 (P3) eV. The present oxygen at XPS spectrum peaks corresponded to chemisorbed surface oxygen and water (P1), surface adsorbed OH and/or oxygen vacancy (P2), and O^{2-} (P3) in ZnO lattice.[32] It is worth to say that ratio P2/P3 decreased with the increase of the bilayer thickness, pointing to the improvement of nanolaminates crystallinity and the decrease of the defect concentration.

2. Band Gap Energy Determination. It is well-known that the difference between the onset of inelastic electron losses (E_{loss}) energy and the core level peak (e.g., oxygen peak, E_O 1s) allows one to estimate the energy gap (E_g) of the material.[33] The intersection of the linear-fit line of the measured electron loss spectra near the core level peak and the background "zero" level gives us the onset of inelastic losses occurring in Al_2O_3.[34] Then we can calculate the band gap energy of Al_2O_3 using the formula: $E_g = E_{loss} - E_O$. Applying this theory, we have calculated E_g of Al_2O_3 for PAN-nanolaminate samples (Figure 5). The following values were obtained: 5.37 ± 0.06, 5.78 ± 0.09, 5.88, and 6.01 ± 0.08 eV for PAN-nanolaminate samples with 0.6, 1, 2.6, and 5 nm Al_2O_3 layer thickness, respectively. Unfortunately, it was impossible to calculate the E_g of Al_2O_3 for PAN-Al_2O_3/ZnO (10 nm Al_2O_3 layer thickness) due to the thick top layer of ZnO under the Al_2O_3 layer. Our obtained value of about 6 eV is low compared to the one reported for amorphous Al_2O_3 (8.8 eV).[33] This observation might be explained by the highly defected structure of Al_2O_3 layer in nanolaminates. Upon increasing the Al_2O_3 layer thickness in PAN-nanolaminates, the E_g gradually increases and tends to bulk value.

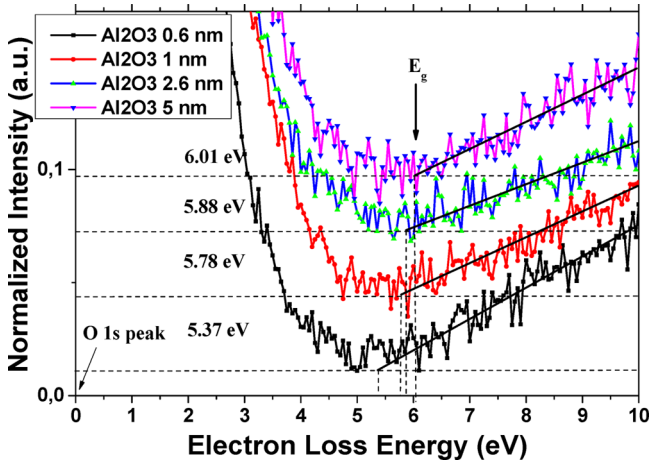

Figure 5. O 1s energy-loss spectra for band gap determination of Al_2O_3 of ZnO/Al_2O_3 nanolaminate coated polymer fiber with different bilayers thicknesses.

3. Work Function Determination. The electronic structure of PAN-ZnO/Al_2O_3 nanolaminates as a function of the bilayer thicknesses was studied with UV photoelectron spectroscopy (UPS) (He I emission 21.22 eV). The work function (Φ) of the ZnO could be estimated by subtracting the secondary electron cutoff value from the He excitation source of 21.22 eV (Φ = 21.22 eV, E_{SEC}). Figure 6 shows the UPS spectra of PAN-ZnO/Al_2O_3 nanolaminates. The calculated values of Φ are shown in the image. The Φ of ZnO decreases gradually from 5.86 eV (20 nm bilayer thickness) to 5.19 eV (1.2 nm bilayer thickness), which is possibly due to the morphology changes of the top ZnO layers in nanolaminates. The structure of ZnO layer in the 20 nm bilayer thickness sample is polycrystalline (TEM results; Figure 1); thus, the energy barriers presenting at the border of disorientated ZnO nanocrystallites increase the value of the Φ. The small peak corresponding to Al_2O_3 is also present in Figure 6. The average value of WF for Al_2O_3 is approximately 4.7 eV, and it changes insignificantly.

Work functions of ZnO and Al_2O_3 layers are plotted in Figure 6. The work function of Al_2O_3 was insignificantly changed whereas the ZnO work function significantly decreased with the bilayer thickness.

The change of Φ could be explained by band bending, formed at the upper layer of the nanolaminates (ZnO−air interface) (Figure 7). Electron affinities of ZnO and Al_2O_3 were taken χ_{ZnO} = 4.37 eV and χ_{Al2O3} = 1.35 eV, respectively.[35,36]

DOI: 10.1021/acs.jpcc.5b12263
J. Phys. Chem. C 2016, 120, 5124−5132

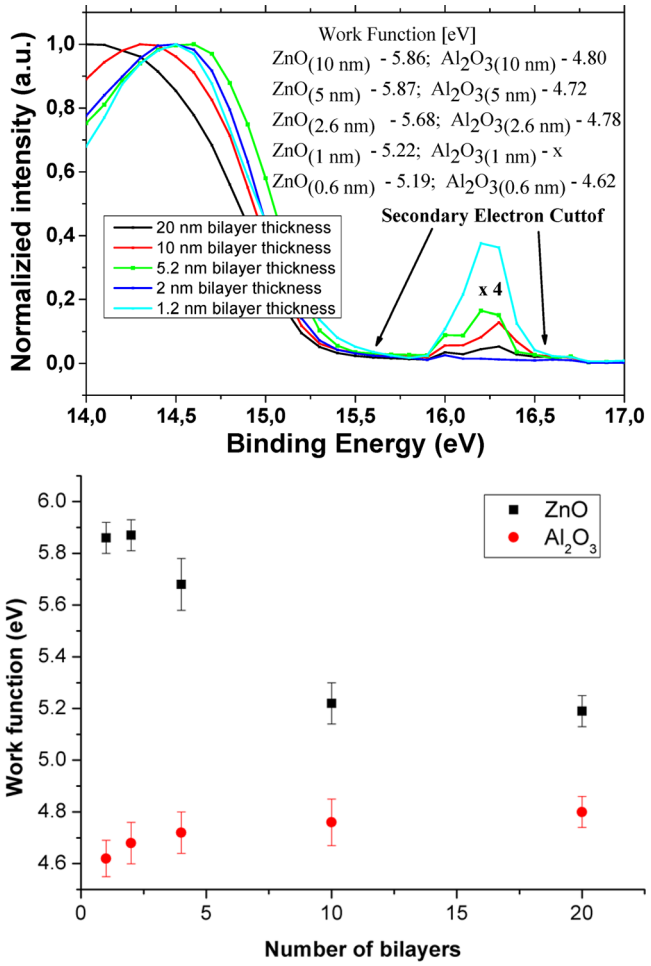

Figure 6. UPS results of work function measurements of ZnO/Al_2O_3 nanolaminate coated polymer fiber with different bilayer thicknesses.

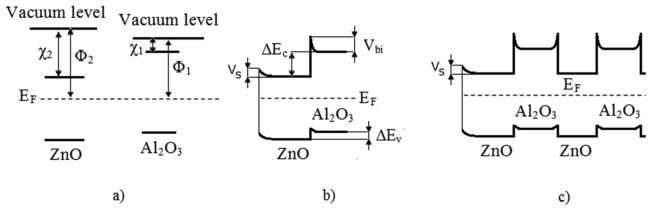

Figure 7. Zone diagram of Al_2O_3/ZnO nanolaminate formation: (a) single layers before contact, (b) 1 bilayer, and (c) n bilayers.

Fermi level E_F position in each component of the nanolaminates was estimated:

$$E_F = \Phi - \chi \quad (1)$$

where Φ is the work function.

The conductance band and valence band gap offsets could be calculated as (Table 2):

$$\Delta E_c = \chi_2 - \chi_1 \quad (2)$$

$$\Delta E_v = E_{g1} - E_{g2} - \Delta E_c \quad (3)$$

where $E_{g1,2}$ and $\chi_{1,2}$ are band gap values of Al_2O_3 and ZnO and electron affinity values of ZnO and Al_2O_3, respectively.

The built in potential V_{bi} between two altering ZnO and Al_2O_3 layers was calculated due to (Table 2):

$$V_{bi}q = E_{F2} - E_{F1} \quad (4)$$

where q is an electron charge, and E_{F1} and E_{F2} are Fermi level positions in Al_2O_3 and ZnO, correspondently.

To estimate potential drops in ZnO and Al_2O_3, the Debye lengths in the altering materials were estimated:

$$L_D = \sqrt{\frac{kT\varepsilon\varepsilon_0}{N_d q}} \quad (5)$$

where k, T, ε, and ε_0 are the Boltzmann's constant, absolute temperature, dielectric permittivity of ZnO (ε = 8.5), and electric constant ($\varepsilon_0 = 8.85 \times 10^{-12}$ F m^{-1}), respectively. The donor concentrations in ZnO and Al_2O_3 were taken as 10^{23} and 10^{16} m^{-3}, respectively.[37,38] The estimated Debye lengths were 10^{-8} and 5×10^{-5} m for ZnO and Al_2O_3, respectively.

The potential drops in ZnO and Al_2O_3 could be calculated as

$$V_{ZnO} = L_{DZnO}\frac{V_{bi}}{L_{DAl2O3} + L_{DZnO}}$$

$$V_{Al2O3} = V_{bi} - V_{ZnO} \quad (6)$$

Based on eqs 5 and 6, the potential drop in ZnO was 10^{-4} eV. Therefore, the band bending in ZnO at the interface between ZnO and Al_2O_3 is significantly small and the potential drop will be mostly faced in Al_2O_3 layer.

The estimated values of ZnO work function are strongly affected by the surface band bending in the upper ZnO layer. The later could be estimated from eq 7:

$$V_s = \Phi_{1bl} - \Phi_{20bl} \quad (7)$$

where Φ_{1bl} and Φ_{20bl} are the work function of ZnO in 1 bilayer and 20 bilayer samples, respectively. The obtained V_s value was 0.64 eV. The depletion width in ZnO could be calculated from eq 8:[39]

$$W = \sqrt{\frac{2V_s\varepsilon\varepsilon_0}{qN_d}} \quad (8)$$

The estimated W value was around 50 nm. Therefore, the upper ZnO layer will be fully depleted and a double barrier structure will be formed on the borders of the ZnO layers, pointing to the confinement of the electrons in ZnO along Z-axis. The observed change of work function in ZnO layers results from the presence of hydroxyl and oxygen groups, adsorbed on ZnO surface. This is corroborated by the band at 3500 cm^{-1} observed in FTIR and XPS analysis. The change of the work function with the increase of the bilayer numbers is

Table 2. Electronic parameters of Al_2O_3/ZnO Ultrathin Nanolaminate Synthesis by ALD[a]

	electron affinity (eV)	band gap (eV)	work function (eV)	ΔE_c (eV)	ΔE_v (eV)	V_{bi} (eV)
Al_2O_3	1.35 [ref 36]	6 ± 0.1	4.8 ± 0.1	3	0.3 ± 0.1	2 ± 0.1
ZnO	4.35 [ref 35]	3.3 [ref 35]	5.8 ± 0.1			

[a]Numbers in square parentheses are references.

DOI: 10.1021/acs.jpcc.5b12263
J. Phys. Chem. C 2016, 120, 5124−5132

affected by 'screening' of the induced electric field on the surface of the middle Al_2O_3 layers. The part of the depleted ZnO layers will decrease and therefore, the average value of the work function will decrease.

4. Photoluminescence of PAN-Al_2O_3/ZnO Nanolaminates. The photoluminescence of the PAN-Al_2O_3/ZnO nanolaminates samples showed intense broad visible emission (Figure 8). The deconvolution of the peaks was performed

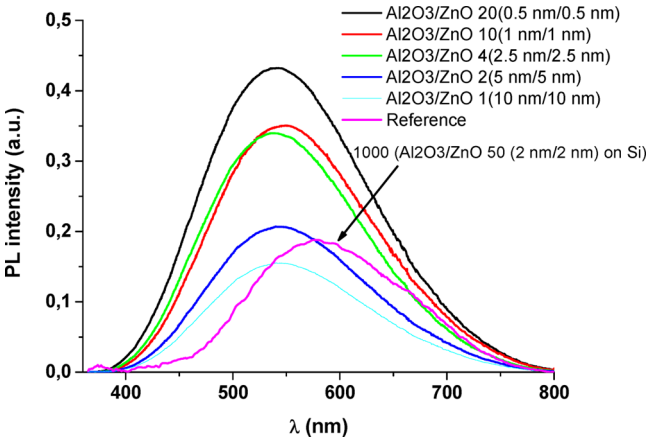

Figure 8. Room temperature PL spectra of PAN-Al_2O_3/ZnO nanolaminates with different bilayer thicknesses; Al_2O_3/ZnO nanolaminate 50 (2 nm × 2 nm) deposited on silicon was added for comparison.

using Gaussian fitting (Supporting Information; Figure SI4). Peaks at 473, 520, and 580 nm have been found. In ZnO, PL appears due to the photogenerated holes and electrons as the equilibrium holes concentration is too low. PL depends on the defects concentration. The visible PL intensity increases with the decrease of the layer thickness due to the growth of defects number. It was shown that PAN, as a template, induces the nucleation of pure ZnO during the growth affecting the optical properties.[20] However, in the present work, PAN template did not influence the PL of ZnO as since Al_2O_3 layer was the first layer deposited over PAN in all the analyzed samples. It is known that PL of ZnO is sensitive to surface band bending and grain size dimensions.[3] Due to the depleted layer, no exciton emission was observed in the samples with 20, 10, and 5.2 nm bilayers thicknesses. Moreover, the strong visible emission has been observed for all samples. The intensity of the measured emission was 1000-fold higher than the PL emission of the nanolaminates, deposited on Si substrates.[1,20] The significant increase of the PL was found with the increase of the bilayer numbers. It has been reported that visible PL in ZnO nanostructures is resulted from defects, mostly from Zn and O vacancies and interstitials.[1,3,20] According to that, the observed peaks at 473, 520, and 580 nm could be assigned to neutral, single charged and double charged oxygen vacancies, respectively.[1,3,20] However, the peak at 473 nm could also be related to Zn vacancies.[1,3,20] Measuring only room temperature luminescence, we cannot discriminate the observed peak at 473 nm between two different defect states. However, this fact does not change the nature of the emission.

According to XPS data, the number of defects decreased with an increase of the bilayer thickness. Therefore, the 1.2 nm bilayer thickness sample showed the highest photoluminescence. The work function measurements of the samples showed the significant influence of the surface band bending in the upper ZnO layer. The band bending could stimulate the separation of photogenerated electrons and holes, increasing a role of nonirradiative transitions. As shown above, the Al_2O_3 layers "screen" the influence of the surface charge in the upper layer and form heterostructures in which ZnO layers are electron-rich. Besides the decrease of the average value of ZnO work function, the increase of the emission intensity occurred.

The work function of ZnO is related to a width of the space charge and band bending.[40,41] The change of WF can point to the adsorption/desorption, interface forming and other changes on the surface. In our case, WF demonstrates that the band bending decreases when more Al_2O_3 layers are introduced in the nanolaminates which induced the electron-rich area in ZnO. It is one of the factors which influences PL value.

In our previous works,[1,3] we observed similar results when no excitonic peaks were found for thin layers due to band bending and low grain size. This will result from the high concentration of defects, the low grain size (compatible with exciton Bohr radius for ZnO (2.6 nm)), and the surface band bending. Therefore, domination of defect level emission and low rate of exciton formation are observed.

The ZnO layers were polycrystalline with small grain size. We suppose that the grain boundaries will have the following effects in the optical properties of the nanolaminates: (i) Quantum confinement effect: due to the low grain size, the blue shift of the band gap is observed. (ii) Defects are formed on the grain boundaries:[42] XPS showed the higher concentration of the defects for low ZnO thickness, which enhanced visible photoluminescence. (iii) Grain boundaries influence light absorption, particularly, the Urbach tail:[42] a higher Urbach tail value is observed for low ZnO thickness due to the increasing of the grain boundaries active surface (more defects). In the present study, we have shown that the ZnO work function significantly decreased with the decreasing of the bilayer thickness. We explain this observation by band bending. It is well-known fact that grain boundaries can induce localized energy states within the band gap, leading to trapped, localized charges. These will form an electrostatic potential barrier, band bending, for the majority of carrier transport across grain boundaries and as well as enhanced recombination of photogenerated carriers, thus increasing the PL what we can observe on the PL spectra. Many other authors have shown that the formation of a nanocrystalline structure decreases the electron work function.[43,44]

■ CONCLUSION

Summarizing, the structural and optical properties of Al_2O_3/ZnO determined from the XPS, TEM, FTIR, XRD and PL analysis provide an important information about crystalline structure of nanolaminates on the 1D PAN substrate. The amorphous-to crystalline transition has been observed for ZnO nanolayers at the thickness of 2.6 nm on the 1D PAN nanotemplate. In particular, strong influence of the bilayer thicknesses on the crystallinity of ZnO nanolayers has been found. Due to the quantum confinement effect, the shift of XPS peaks to higher energies has been observed. Work function of Al_2O_3 was mostly independent of the bilayers number whereas the ZnO work function decreased with an increase of the bilayer number. The observed phenomenon indicate surface band bending on the upper layer of ZnO and further charge "screening" by Al_2O_3 layers in internal ZnO layers of the nanolaminates.

DOI: 10.1021/acs.jpcc.5b12263
J. Phys. Chem. C 2016, 120, 5124−5132

Photoluminescence of the nanolaminates corresponded to emission bands in ZnO nanolayers. Due to low grain size, high defect concentration, and surface band bending, no excitonic peaks were observed. The defect emission band was affected by the band bending and defect concentration. The observed XPS and PL data are in good correlation. The enhanced PL of the nanolaminates could be used for optical (bio)sensing.

■ ASSOCIATED CONTENT

Supporting Information

The Supporting Information is available free of charge on the ACS Publications website at DOI: 10.1021/acs.jpcc.5b12263.

Deconvolution of XPS and PL peaks, TEM and EDX/TEM mapping (PDF)

■ AUTHOR INFORMATION

Corresponding Authors

*E-mail: roman.viter@lu.lv. Phone: +37120058754.
*E-mail: igoyat@amu.edu.pl. Phone: +48731308173.
*E-mail: mikhael.bechelany@univ-montp2.fr. Phone: +33467149167. Fax: +33467149119.

Notes

The authors declare no competing financial interest.

■ ACKNOWLEDGMENTS

This work was partially supported by the EU under BIOSENSORS-AGRICULT, Contract PIRSES-GA-2012-318520 "Development of Nanotechnology-based Biosensors for Agriculture", "Nanomaterials and their application to biomedicine" (Contract Number PBS1/A9/13/2012), and "FOTONIKA-LV-FP7-REGPOT-CT-2011" (Contract Number 285912). The authors would like to acknowledge the "Institut Européen des Membranes (IEM)-UMR CNRS 5635" which partially supports this study through the project "Axe-health/P1S-2014". This study was partially supported by the ANR project ANR-14-CE07-0011 "BONALD".

■ REFERENCES

(1) Chaaya, A.; Viter, R.; Baleviciute, I.; Bechelany, M.; Ramanavicius, A.; Gertnere, Z.; Erts, D.; Smyntyna, V.; Miele, P. Tuning Optical Properties of Al_2O_3/ZnO Nanolaminates Synthesized by Atomic Layer Deposition. *J. Phys. Chem. C* **2014**, *118*, 3811−3819.

(2) Raghavan, R.; Bechelany, M.; Parlinska, M.; Frey, D.; Mook, W. M.; Beyer, A.; Michler, J.; Utke, I. Nanocrystalline-to-Amorphous Transition in Nanolaminates Grown by Low Temperature Atomic Layer Deposition and Related Mechanical Properties. *Appl. Phys. Lett.* **2012**, *100*, 191912.

(3) Abou Chaaya, A.; Viter, R.; Bechelany, M.; Alute, Z.; Erts, D.; Zalesskaya, A.; Kovalevskis, K.; Rouessac, V.; Smyntyna, V.; Miele, P. Evolution of Microstructure and Related Optical Properties of ZnO Grown by Atomic Layer Deposition. *Beilstein J. Nanotechnol.* **2013**, *4*, 690−698.

(4) Marichy, C.; Bechelany, M.; Pinna, N. Atomic Layer Deposition of Nanostructured Materials for Energy and Environmental Applications. *Adv. Mater.* **2012**, *24*, 1017−1032.

(5) Bechelany, M.; Balme, S.; Miele, P. Atomic Layer Deposition of Biobased Nanostructured Interfaces for Energy, Environmental and Health Applications. *Pure Appl. Chem.* **2015**, *87*, 751−758.

(6) Abou Chaaya, A.; Le Poitevin, M.; Cabello-Aguilar, S.; Bechelany, M.; Balme, S.; Balanzat, E.; Janot, J.-M.; Pochat-Bohatier, C.; Miele, P.; Dejardin, P. Enhanced Ionic Transport Mechanism by Gramicidin a Confined inside Nanopores Tuned by Atomic Layer Deposition. *J. Phys. Chem. C* **2013**, *117*, 15306−15315.

(7) Cabello-Aguilar, S.; Balme, S.; Abou Chaaya, A.; Bechelany, M.; Balanzat, E.; Janot, J.-M.; Pochat-Bohatier, C.; Miele, P.; Dejardin, P. Slow Translocation of Polynucleotides and Their Discrimination by Alpha-Hemolysin inside a Single Track-Etched Nanopore Designed by Atomic Layer Deposition. *Nanoscale* **2013**, *5*, 9582−9586.

(8) Elam, J. W.; Sechrist, Z. A.; George, S. M. ZnO/Al_2O_3 Nanolaminates Fabricated by Atomic Layer Deposition: Growth and Surface Roughness Measurements. *Thin Solid Films* **2002**, *414*, 43−55.

(9) Karvonen, L.; Säynätjoki, A.; Chen, Y.; Jussila, H.; Rönn, J.; Ruoho, M.; Alasaarela, T.; Kujala, S.; Norwood, R. A.; Peyghambarian, N.; et al. Enhancement of the Third-Order Optical Nonlinearity in ZnO/ Al_2O_3 Nanolaminates Fabricated by Atomic Layer Deposition. *Appl. Phys. Lett.* **2013**, *103*, 031903.

(10) Banerjee, P.; Lee, W.-J.; Bae, K.-R.; Lee, S. B.; Rubloff, G. W. Structural, Electrical, and Optical Properties of Atomic Layer Deposition Al-Doped Zno Films. *J. Appl. Phys.* **2010**, *108*, 043504.

(11) Viter, R.; Baleviciute, I.; Abou Chaaya, A.; Mikoliunaite, L.; Balevicius, Z.; Ramanavicius, A.; Zalesska, A.; Vataman, V.; Smyntyna, V.; Gertnere, Z.; et al. Optical Properties of Ultrathin Al_2O_3/ZnO Nanolaminates. *Thin Solid Films* **2015**, *594*, 96−100.

(12) Moret, M.; Abou Chaaya, A.; Bechelany, M.; Miele, P.; Robin, Y.; Briot, O. Atomic Layer Deposition of Zinc Oxide for Solar Cell Applications. *Superlattices Microstruct.* **2014**, *75*, 477−484.

(13) Kayaci, F.; Ozgit-Akgun, C.; Donmez, I.; Biyikli, N.; Uyar, T. Polymer-Inorganic Core-Shell Nanofibers by Electrospinning and Atomic Layer Deposition: Flexible Nylon-Zno Core-Shell Nanofiber Mats and Their Photocatalytic Activity. *ACS Appl. Mater. Interfaces* **2012**, *4*, 6185−6194.

(14) Kemnade, N.; Shearer, C. J.; Dieterle, D. J.; Cherevan, A. S.; Gebhardt, P.; Wilde, G.; Eder, D. Non-Destructive Functionalisation for Atomic Layer Deposition of Metal Oxides on Carbon Nanotubes: Effect of Linking Agents and Defects. *Nanoscale* **2015**, *7*, 3028−3034.

(15) Lin, Y.-H.; Lee, P.-S.; Hsueh, Y.-C.; Pan, K.-Y.; Kei, C.-C.; Chan, M.-H.; Wu, J.-M.; Perng, T.-P.; Shih, H. C. Atomic Layer Deposition of Zinc Oxide on Multiwalled Carbon Nanotubes for UV Photodetector Applications. *J. Electrochem. Soc.* **2011**, *158*, K24−K27.

(16) Oldham, C. J.; Gong, B.; Spagnola, J. C.; Jur, J. S.; Senecal, K. J.; Godfrey, T. A.; Parsons, G. N., Atomic Layer Deposition on Polymers: Applications to Physical Encapsulation of Electrospun Nylon Nanofibers. In *ECS Trans.*, Elam, J. W.; DeGendt, S.; VanDerStraten, O.; Delabie, A.; Londergan, A.; Bent, S. F.; Roozeboom, F., Eds. **2010**; Vol. *33*, pp 279−290.

(17) Stano, K. L.; Carroll, M.; Padbury, R.; McCord, M.; Jur, J. S.; Bradford, P. D. Conformal Atomic Layer Deposition of Alumina on Millimeter Tall, Vertically-Aligned Carbon Nanotube Arrays. *ACS Appl. Mater. Interfaces* **2014**, *6*, 19135−19143.

(18) Shi, Y.; Li, Y.; Zhang, J.; Yu, Z.; Yang, D. Electrospun Polyacrylonitrile Nanofibers Loaded with Silver Nanoparticles by Silver Mirror Reaction. *Mater. Sci. Eng., C* **2015**, *51*, 346−355.

(19) Chaaya, A.; Bechelany, M.; Balme, S.; Miele, P. Zno 1D Nanostructures Designed by Combining Atomic Layer Deposition and Electrospinning for UV Sensor Applications. *J. Mater. Chem. A* **2014**, *2*, 20650−20658.

(20) Viter, R.; Chaaya, A.; Iatsunskyi, I.; Nowaczyk, G.; Kovalevskis, K.; Erts, D.; Miele, P.; Smyntyna, V.; Bechelany, M. Tuning of Zno 1D Nanostructures by Atomic Layer Deposition and Electrospinning for Optical Gas Sensor Applications. *Nanotechnology* **2015**, *26*, 105501.

(21) Ismaila, A. F.; Mustafa, A.; Abd. Rahaman, M. S. Effect of Blending Temperature on the Characteristics of Modified Polyacrylonitrie Homopolymer. *Mod. Appl. Sci.* **2009**, *2*, 131−141.

(22) Zacharias, M.; Streitenberger, P. Crystallization in the Limit of Ultra Thin Layers- a New Crystallization Model. *MRS Online Proc. Libr.* **2000**, *638*, F6.2.1.

(23) Iatsunskyi, I.; Kempinski, M.; Nowaczyk, G.; Jancelewicz, M.; Pavlenko, M.; Zaleski, K.; Jurga, S. Structural and XPS Studies of PSi/TiO_2 Nanocomposites Prepared by ALD and Ag- Assisted Chemical Etching. *Appl. Surf. Sci.* **2015**, *347*, 777−783.

(24) Briggs, D. *Handbook of X-Ray Photoelectron Spectroscopy* Wanger, C. D., Riggs, W. M.; Davis, L. E., Moulder, J. F., Muilenberg, G. E.

DOI: 10.1021/acs.jpcc.5b12263
J. Phys. Chem. C 2016, 120, 5124−5132

Perkin-Elmer Corp., Physical Electronics Division: Eden Prairie, MN, 1979; 190 pp. $195. *Surf. Interface Anal.* 1981, *3*, DOI: 10.1002/sia.740030412.
(25) Mosquera, A. A.; Horwat, D.; Rashkovskiy, A.; Kovalev, A.; Miska, P.; Wainstein, D.; Albella, J. M.; Endrino, J. L. Exciton and Core-Level Electron Confinement Effects in Transparent Zno Thin Films. *Sci. Rep.* **2013**, *3*, 1714.
(26) Das, J.; Pradhan, S. K.; Sahu, D. R.; Mishra, D. K.; Sarangi, S. N.; Nayak, B. B.; Verma, S.; Roul, B. K. Micro-Raman and Xps Studies of Pure ZnO Ceramics. *Phys. B* **2010**, *405*, 2492−2497.
(27) De la Rosa, E.; Sepúlveda-Guzman, S.; Reeja-Jayan, B.; Torres, A.; Salas, P.; Elizondo, N.; Yacaman, M. J. Controlling the Growth and Luminescence Properties of Well-Faceted ZnO Nanorods. *J. Phys. Chem. C* **2007**, *111*, 8489−8495.
(28) Wang, H.; Baek, S.; Song, J.; Lee, J.; Lim, S. Microstructural and Optical Characteristics of Solution-Grown Ga-Doped ZnO Nanorod Arrays. *Nanotechnology* **2008**, *19*, 075607.
(29) Wang, H.; Xie, C. The Effects of Oxygen Partial Pressure on the Microstructures and Photocatalytic Property of Zno Nanoparticles. *Phys. E* **2008**, *40*, 2724−2729.
(30) Kovalev, A. I.; Wainstein, D. L.; Rashkovskiy, A. Y.; Osherov, A.; Golan, Y. Size Shift of Xps Lines Observed from Pbs Nanocrystals. *Surf. Interface Anal.* **2010**, *42*, 850−854.
(31) Sharma, A.; Singh, B. P.; Dhar, S.; Gondorf, A.; Spasova, M. Effect of Surface Groups on the Luminescence Property of ZnO Nanoparticles Synthesized by Sol-Gel Route. *Surf. Sci.* **2012**, *606*, L13−L17.
(32) Zhang, X.; Qin, J.; Xue, Y.; Yu, P.; Zhang, B.; Wang, L.; Liu, R. Effect of Aspect Ratio and Surface Defects on the Photocatalytic Activity of ZnO Nanorods. *Sci. Rep.* **2014**, *4*, 4596.
(33) Nichols, M. T.; Li, W.; Pei, D.; Antonelli, G. A.; Lin, Q.; Banna, S.; Nishi, Y.; Shohet, J. L. Measurement of Bandgap Energies in Low-K Organosilicates. *J. Appl. Phys.* **2014**, *115*, 094105.
(34) Iatsunskyi, I.; Kempinski, M.; Jancelewicz, M.; Zaleski, K.; Jurga, S.; Smyntyna, V. Structural and Xps Characterization of ALD Al_2O_3 Coated Porous Silicon. *Vacuum* **2015**, *113*, 52−58.
(35) Ozawa, K.; Sawada, K.; Shirotori, Y.; Edamoto, K.; Nakatake, M. Angle-Resolved Photoelectron Spectroscopy Study of the Anion-Derived Dangling-Bond Band on ZnO(1010). *Phys. Rev. B: Condens. Matter Mater. Phys.* **2003**, *68*, 125417.
(36) Ren, J.; Li, B.; Zheng, J.-G.; Liu, J. High-Density NiSi Nanocrystals Embedded in Al_2O_3/SiO_2 Double-Barrier for Robust Retention of Nonvolatile Memory. *Solid-State Electron.* **2012**, *67*, 23−26.
(37) Maragliano, C.; Lilliu, S.; Dahlem, M. S.; Chiesa, M.; Souier, T.; Stefancich, M. Quantifying Charge Carrier Concentration in ZnO Thin Films by Scanning Kelvin Probe Microscopy. *Sci. Rep.* **2014**, *4*, 4203.
(38) Medvedev, D. A.; Rybinskaya, A. A.; Kenzhin, R. M.; Volodin, A. M.; Bedilo, A. F. Characterization of Electron Donor Sites on Al_2O_3 Surface. *Phys. Chem. Chem. Phys.* **2012**, *14*, 2587−2598.
(39) Liao, Z.-M.; Zhang, H.-Z.; Zhou, Y.-B.; Xu, J.; Zhang, J.-M.; Yu, D.-P. Surface Effects on Photoluminescence of Single ZnO Nanowires. *Phys. Lett. A* **2008**, *372*, 4505−4509.
(40) Lin, Y.-J.; Tsai, C.-L., Changes in Surface Band Bending, Surface Work Function, and Sheet Resistance of Undoped ZnO Films Due to $(NH_4)_2S_X$ Treatment. *J. Appl. Phys.* **2006**, *100*.11372110.1063/1.2399894
(41) Schlesinger, R.; Xu, Y.; Hofmann, O. T.; Winkler, S.; Frisch, J.; Niederhausen, J.; Vollmer, A.; Blumstengel, S.; Henneberger, F.; Rinke.; et al. Controlling the Work Function of Zno and the Energy-Level Alignment at the Interface to Organic Semiconductors with a Molecular Electron Acceptor. *Phys. Rev. B: Condens. Matter Mater. Phys.* **2013**, *87*, 155311.
(42) Kumar, S.; Asokan, K.; Singh, R. K.; Chatterjee, S.; Kanjilal, D.; Ghosh, A. K. Investigations on Structural and Optical Properties of ZnO and ZnO:Co Nanoparticles under Dense Electronic Excitations. *RSC Adv.* **2014**, *4*, 62123−62131.
(43) Sadewasser, S.; Glatzel, T.; Schuler, S.; Nishiwaki, S.; Kaigawa, R.; Lux-Steiner, M. C. Kelvin Probe Force Microscopy for the Nano Scale Characterization of Chalcopyrite Solar Cell Materials and Devices. *Thin Solid Films* **2003**, *431*, 257−261.
(44) Jiang, C. S.; Noufi, R.; AbuShama, J. A.; Ramanathan, K.; Moutinho, H. R.; Pankow, J.; Al-Jassim, M. M. Local Built-in Potential on Grain Boundary of $Cu(In,Ga)Se_2$ Thin Films. *Appl. Phys. Lett.* **2004**, *84*, 3477−3479.

DOI: 10.1021/acs.jpcc.5b12263
J. Phys. Chem. C 2016, 120, 5124−5132